

Accurate interpolation methods for the annual simulation of solar central receiver systems using celestial coordinate system

P. Richter^{a,*}, J. Tinnes^b, L. Aldenhoff^b

^a Karlsruhe Institute of Technology (KIT), Steinbuch Centre for Computing, Hermann-von-Helmholtz-Platz 1, 76344 Eggenstein-Leopoldshafen, Germany

^b RWTH Aachen University, Research Group for Theory of Hybrid Systems, Department of Computer Science, Ahornstr. 55, 52074 Aachen, Germany

ARTICLE INFO

Keywords:

Solar central receiver system
Annual simulation
Ecliptic coordinate system
Equatorial coordinate system
Celestial coordinate system

ABSTRACT

Heliostat field layout optimization bases on simulations of the annual energy production. To reduce the computation time of the optimization process, one can try to reduce the number of simulation points of the annual domain, while keeping similar accuracy. For the temporal domain, there exist already different approaches as aggregation of days. To further reduce the number of needed simulation points, in this paper we decouple the power computation from the irradiation, such that we just regard the computation of the power plant efficiency. This time-dependent parameter is transformed into a celestial coordinate system where the solar angle-dependent efficiency will be approximated using suitable multi-dimensional interpolation methods.

We distinguish between an accurate approximation of the received annual optical energy and the electrical energy of each moment of a year. These methods are demonstrated for the existing heliostat field layouts PS10 and Gemasolar in Seville, while using realistic weather conditions. With this new approach just around 40 simulation points suffice to reach an accuracy of 99.9% for the received power for smaller power plants as PS10, and for larger plants as Gemasolar. Compared to a state-of-the-art method, this investigation helps to accelerate the simulation by factor three.

1. Introduction

Solar central receiver systems consist of a high tower, surrounded by many heliostats, which reflect the sun rays to the receiver mounted on top of the tower. The arriving solar energy is converted into thermal energy by heating up a fluid, e.g. water, air or molten salt. This hot fluid is used to generate steam, such that electricity is generated with the help of a steam turbine and a generator.

For heliostat field layout optimization an accurate model is needed, which computes the annual energy production on the basis of simulating the produced power at different moments (instances of time or sun positions) throughout the whole year. In general, the simulation of a single moment is done with a raytracer tool, such as STRAL, SolTrace, HelioSim or Tonatiuh (Ahlbrink et al., 2012; Wendelin, 2003; Potter et al., 2018; Blanco et al., 2005).

As the reduction of the simulation effort due to a reduced number of time points linearly influences the CPU run-time of the annual simulation, it is advantageous to reduce the number of needed moment

simulations while keeping similar accuracy for the annual energy production. In the following, existing methods to select the moments throughout a year are presented.

1.1. State of the art

Due to similar sun positions on neighboring days, a single representative moment can be used. A popular approach for the discretization is to use every hour of the 21st of each month as simulation point. Considering the symmetry of one year around the 21st of June, just seven months are regarded such that here only around 72 points need to be simulated (Pitz-Paal et al., 2011). Noone et al. (2012) follow the monthly approach, but choose the original hourly moments on the basis of the daily sun path in the horizontal celestial coordinate system¹, which results in non-equidistant temporal points. As these points are regarded as reference for the neighboring region, the approximation method belongs to the group of nearest neighbor approaches.

As these approaches have mainly been developed for clear-sky meteorological data, an extension is needed for realistic

* Corresponding author.

E-mail address: pascal.richter@kit.edu (P. Richter).

¹ The horizontal celestial coordinate system is defined by the solar azimuth γ and solar elevation α .

Nomenclature	
d	Day of a year
t	Time [hours]
ϕ	Latitude of the location [°]
γ	Solar azimuth angle [°]
α	Solar elevation angle [°]
δ	Solar declination angle [°]
ω	Solar hour angle [°]
λ	Solar ecliptic longitude [°]
A_{helios}	Mirror area of the heliostat field [m ²]
I_{DNI}	Direct normal solar irradiation [W/m ²]
P^{sim}	Simulated optical power [W]
P^{approx}	Approximated optical power [W]
$E_{\text{year}}^{\text{sim}}$	Simulated annual energy production [Wh]
$E_{\text{year}}^{\text{approx}}$	Approximated annual energy production [Wh]
η^{sim}	Simulated optical efficiency
η^{approx}	Approximated optical efficiency
ϵ_{AEP}	Relative error of the optical annual energy production
ϵ_{rmse}	Root-mean-squared error for received power for each time point in a year

meteorological data², due to the volatile direct normal solar irradiation I_{DNI} , compare Fig. 1 (a) and (b). Richter et al. (2018b) propose to aggregate the solar irradiation of neighboring moments to receive accurate approximations while using realistic meteorological data. Another approach for considering realistic weather conditions is proposed by Schöttl et al. (2016), where the power computation is decoupled from the solar irradiation, such that just the optical simulation of the power plant efficiency is regarded. Then, for each instance of time, the realistic weather data is used and coupled with the efficiency value, which can be approximated by appropriate interpolation methods between simulated efficiency values. The moments are chosen in the horizontal coordinate system. But as the shape of the annual sun path within this coordinate system depends on the location on Earth, see Fig. 2, this method needs carefully be adapted for different sites, such that still the same accuracy can be achieved. Grigoriev et al. (2016) propose to use the ecliptic coordinate system³. For clear-sky meteorological data the symmetry of the seasons and the symmetry within each day was used for the reduction of needed simulation points.

For heliostat field layout optimizations, which consider the optics and the whole thermodynamic cycle including the storage, a method is needed which accurately approximates the received power for each hour in the year. Moreover, the accuracy of the approximation method should be adjustable via its resolution, such that it can be used for dynamic optimization strategies. Furthermore, the approximation method should generally be applicable for any location on Earth from the tropics to the moderate climatic zone in the northern and southern hemisphere, which includes the interesting regions for solar central receiver systems.

In this paper, we use the idea of approximating the optical efficiency and combine it with the suggestion of Grigoriev et al. to operate in a different celestial coordinate system. Thus, we will consider the ecliptic and equatorial⁴ domain and investigate the use of different approximation methods for the optical efficiency.

² EnergyPlus weather file <https://energyplus.net/weather>

³ The ecliptic coordinate system is defined by the ecliptic longitude λ and the hour angle ω .

⁴ The equatorial coordinate system is defined by the solar declination angle δ and the hour angle ω .

1.2. Outline

In Section 2 we introduce the annual simulation methodology, where we decouple the power computation from the irradiation. The underlying temporal domain of the optical efficiency is then transformed into the ecliptic and the equatorial coordinate system, see Section 3. In Section 4, the domains are discretized and suitable interpolation methods are presented. The accuracy of the methods are demonstrated against the PS10 and Gemasolar power plants in Seville (Spain), while using realistic weather data, see Section 5. Finally, the results will be discussed, followed by a short conclusion and an outlook to future work in Section 6.

2. Annual simulation methodology

The annual received energy of a solar central receiver system is defined as the temporal integration of the produced power on each day:

$$E_{\text{year}} = \sum_{d=1}^{365} \int_0^{24} P \left(d, t \right) dt = \sum_{d=1}^{365} \int_0^{24} \left(A_{\text{helios}} \cdot \underbrace{I_{\text{DNI}}(d, t)}_{\text{data from weather file}} \cdot \underbrace{\eta(d, t)}_{\text{optical efficiency}} \right) dt. \quad (1)$$

The produced power P at day d and time t is defined as the product of the total mirror area A_{helios} , the direct normal solar irradiation I_{DNI} and the optical efficiency η . While A_{helios} is constant and I_{DNI} is given by meteorological data, the optical efficiency η needs to be simulated and considers the cosine effect η_{cos} , shading and blocking η_{sb} , the heliostat reflectivity η_{sim} , the atmospheric attenuation η_{aa} and the spillage losses η_{spl} (Richter, 2017):

$$\eta(d, t) = \eta_{\text{cos}}(d, t) \cdot \eta_{\text{sb}}(d, t) \cdot \eta_{\text{sim}}(d, t) \cdot \eta_{\text{aa}}(d, t) \cdot \eta_{\text{spl}}(d, t). \quad (2)$$

As in general the resolution of a typical meteorological year (TMY) is on an hourly basis, the integral over the day in (1) is approximated by the midpoint rule. The resulting annual energy $E_{\text{year}}^{\text{sim}}$ is used as reference, which bases on the simulated reference power $P^{\text{sim}}(d, t)$ with total optical efficiency $\eta^{\text{sim}}(d, t)$ for all sun hours in a year. To reduce computational time, the optical efficiency $\eta(d, t)$ is approximated by $\eta^{\text{approx}}(d, t)$, which results in an approximated optical power $P^{\text{approx}}(d, t)$ and an approximated annual energy production $E_{\text{year}}^{\text{approx}}$. Therefore, we transform the temporal domain to the ecliptic and equatorial coordinate system and use interpolation methods on the basis of a number of simulation points. For their approximation we follow two different objectives, depending on the goal of the heliostat field layout optimization:

- For an accurate approximation of the received annual optical energy, we aim to minimize the relative error of the optical annual energy production (AEP),

$$\epsilon_{\text{AEP}} := \frac{|E_{\text{year}}^{\text{sim}} - E_{\text{year}}^{\text{approx}}|}{E_{\text{year}}^{\text{sim}}}, \quad (3)$$

with $E_{\text{year}}^{\text{sim}}$ as the reference annual energy.

- For an energetic layout optimization (considering the thermal-electrical cycle of a power plant) a precise approximation of the received power for each timepoint in the year is needed. Therefore, we aim on minimizing the root-mean-squared error (RMSE) for a full year, to reduce the deviation at each instance of time,

$$\epsilon_{\text{rmse}} := \sqrt{\frac{1}{|D_{\text{daytime}}|} \sum_{(d,t) \in D_{\text{daytime}}} (P^{\text{sim}}(d, t) - P^{\text{approx}}(d, t))^2}. \quad (4)$$

We restrict the investigation on all time points $(d, t) \in D_{\text{daytime}}$ be-

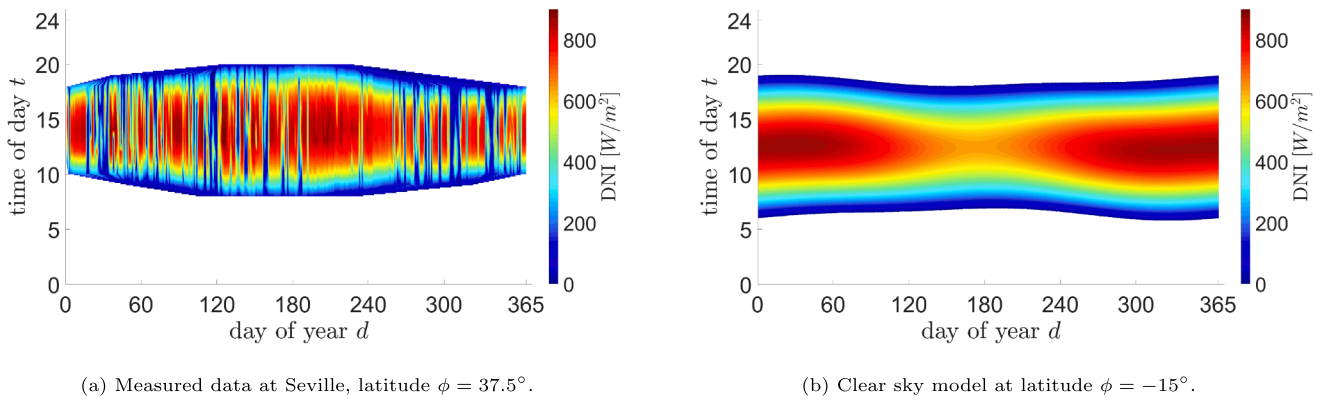


Fig. 1. Direct solar irradiation I_{DNI} in $[\text{W}/\text{m}^2]$ in the temporal domain. For the solar irradiation measured meteorological data from Seville in (a), and clear-sky meteorological data in (b) is used.

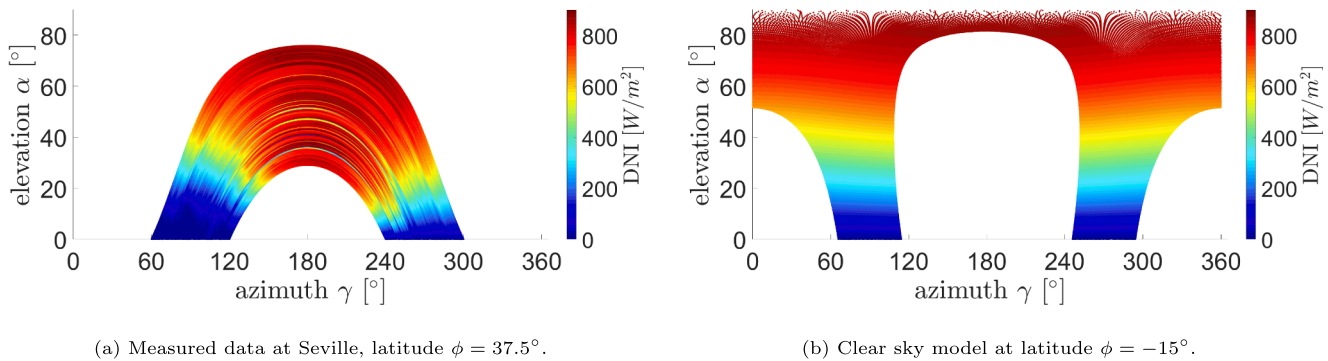


Fig. 2. Annual sun path in the horizontal coordinate system for two locations on Earth with different latitude. For the solar irradiation measured meteorological data from Seville in (a), and clear-sky meteorological data in (b) is used.

tween sunrise and sunset. For example for the measured data in Seville we regard $|D_{\text{daytime}}| = 3789$ out of 8760 hourly time points.

3. Coordinate systems

For a given location on Earth with latitude ϕ and a given date d with time t , the coordinates of the horizontal coordinate system, with solar

3.1. Ecliptic coordinate system

The ecliptic coordinate system uses the Earth as origin, while its primary direction faces towards the vernal equinox⁵, see [Urban and Kenneth Seidelmann \(2013\)](#). The used spherical coordinates under right-hand convention are the ecliptic longitude $\lambda \in [0^\circ, 360^\circ]$ and the hour angle $\omega \in [-180^\circ, 180^\circ]$. By using the Julian date $J_{\text{date}}(d, t)$, the given latitude ϕ of the site and the solar mean anomaly

$$M = \left(357.5291^\circ + 0.98560028^\circ \cdot \left(J_{\text{date}}(d, t) - 2451545 + 0.0008 - \frac{\phi}{360^\circ} \right) \right) \bmod 360^\circ, \tag{5}$$

azimuth γ and solar elevation α can be computed using a sun position algorithm ([Armstrong and Izygon, 2014](#)). These parameters can further

the ecliptic longitude λ is given by [Meeus \(1991\)](#),

$$\lambda = (M + 282.9372^\circ + 1.9148^\circ \cdot \sin(M) + 0.02^\circ \cdot \sin(2M) + 0.0003^\circ \cdot \sin(3M)) \bmod 360^\circ. \tag{6}$$

be transformed in the ecliptic - and equatorial coordinate system.

The hour angle ω describes the angular distance between the solar noon

⁵ The vernal equinox is the position of the sun when it crosses the celestial equator, which is the projection of the Earth's equator to the celestial sphere.

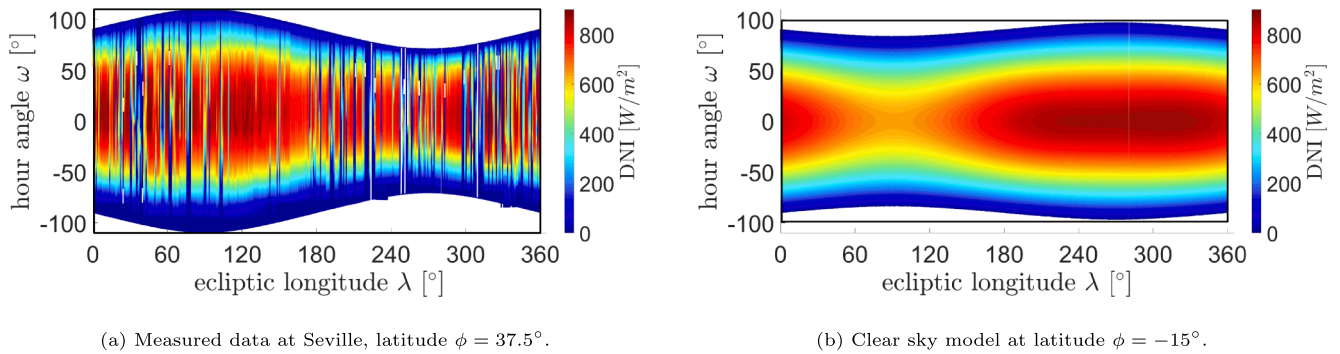


Fig. 3. Annual sun path in the ecliptic coordinate system for two locations on Earth with different latitude. For the solar irradiation, measured meteorological data from Seville in (a), and clear-sky meteorological data in (b) is used. The whole domain can be bounded by a rectangle (black line).

and the sun from the celestial point of view. Thus, it can be interpreted as the time of a day, where it is negative in the morning and positive in the afternoon. By using the given latitude ϕ of the site, the solar azimuth angle γ and the solar elevation angle α , the hour angle is given by

$$\tan(\omega) = \frac{\sin(\gamma)}{\cos(\gamma) \cdot \sin(\phi) + \tan(\alpha) \cdot \cos(\phi)}. \quad (7)$$

Altogether, the region of interest can be bounded by a rectangle, see Fig. 3. While the ecliptic longitude always uses its full interval from 0 to 360 degrees, the used domain of the hour angle depends on the hour angle at sunrise and sunset on the day with the longest period of sunlight of the year d_{long} . Consider that our overall goal is to approximate the optical efficiency, which is needed for the whole domain. As the optical efficiency depends on the power plant configuration, in Fig. 3 just the boundary of the domain and the corresponding DNI is illustrated.

The times for sunrise and sunset for a given day of the year can be computed in dependency of the elevation angle α of the sun (Meeus, 1991). The day with the longest period of sunlight of the year d_{max} depends on the latitude ϕ of the site (Yahyaoui, 2016) and is given by

$$d_{\text{long}} = \begin{cases} d_{\text{JunSolstice}} & , \phi \geq \delta_{\text{max}} \\ \frac{d_{\text{JunSolstice}} + d_{\text{DecSolstice}}}{2} - \frac{365 \cdot \arcsin\left(\frac{\phi}{\delta_{\text{max}}}\right)}{2\pi} & , \delta_{\text{min}} < \phi < \delta_{\text{max}} \\ d_{\text{DecSolstice}} & , \phi \leq \delta_{\text{min}}. \end{cases} \quad (8)$$

with the minimum and maximum obliquity of the ecliptic

$$\delta_{\text{min}} = -23.45^\circ \text{ and } \delta_{\text{max}} = 23.45^\circ. \quad (9)$$

For locations between the tropics this day changes according to the sun’s zenith position, while for locations out of the tropics, this day is the solar summer solstice, the 21st of June on the northern hemisphere and the 21st of December on the southern hemisphere,

$$d_{\text{JunSolstice}} = 172 \text{ and } d_{\text{DecSolstice}} = 355. \quad (10)$$

The shape of the annual sun path for the ecliptic coordinate system does not change much for different locations on Earth, compared to the horizontal coordinate system, compare Figs. 2 and 3. This allows to bound the domain with a simple rectangle. Only the height of the rectangle changes slightly due to the changing range of daily sunlight throughout the year.

3.2. Equatorial coordinate system

The equatorial coordinate system uses also the Earth as origin. But in comparison to the ecliptic coordinate system, the solar declination angle $\delta \in [\delta_{\text{min}}, \delta_{\text{max}}]$ is used instead of the ecliptic longitude λ . The declination angle δ is defined as the angular distance of an object perpendicular to

the celestial equator (Meeus, 1991). It can be computed using the given latitude ϕ of the site, the solar azimuth angle γ and the solar elevation angle α by

$$\sin(\delta) = \sin(\phi)\sin(\alpha) - \cos(\phi)\cos(\alpha)\cos(\gamma). \quad (11)$$

The region of interest can perfectly be bounded by a trapezoid, see Fig. 4. While the solar declination angle always uses its full interval from δ_{min} to δ_{max} , the used domain of the hour angle depends on the hour angle at sunrise and sunset at the day of the June and December solstice, see Eq. (10).

4. Interpolation methods

Within the domain of the ecliptic and equatorial coordinate system, we use suitable multi-dimensional interpolation methods, to approximate the optical efficiency on the basis of chosen simulation points. For the selection of the simulation points the domains are discretized by a regular grid or via Gaussian nodes, while for the interpolation altogether five different approaches are presented.

4.1. Interpolation on regular grid

The interesting region of the domains is bounded by a rectangle or a trapezoid, see Section 3. For the interpolation of the optical efficiency at an arbitrary instance of time, the corresponding point in the (λ, ω) or (δ, ω) domain is transformed into the unit square of the underlying coordinate system, so that finally $P_{xy} := P(x, y) \in [0, 1]^2$, see Fig. 5.

This unit square is sampled with grid points, which represent the simulation points. Thus those points have to be transformed back to the temporal domain. With this we get the simulated power plant efficiency $\eta_{ij}^{\text{sim}} := \eta^{\text{sim}}(x_i, y_j)$ at the grid points (x_i, y_j) for $i = 1, \dots, n$ and $j = 1, \dots, m$. With the simulated optical efficiency $\eta^{\text{sim}}(x, y)$, we can compute the approximated optical efficiency η^{approx} at all arbitrary points using an interpolation method and transform the result back to the original domain. Note that for the ecliptic coordinate system (rectangular domain) the x-axis is the ecliptic longitude which is defined for $\lambda \in [0^\circ, 360^\circ]$. As the first and last column of simulation points represent the same information, just one column of points needs to be simulated.

We considered the following interpolation methods:

- The *nearest-neighbor interpolation method* sets the optical efficiency value of the considered point (x, y) to the same value as of the closest (in Euclidean distance) neighboring point (x_i, y_j) :

$$\eta^{\text{approx}}(x, y) = \eta_{ij}^{\text{sim}}, \quad (12)$$

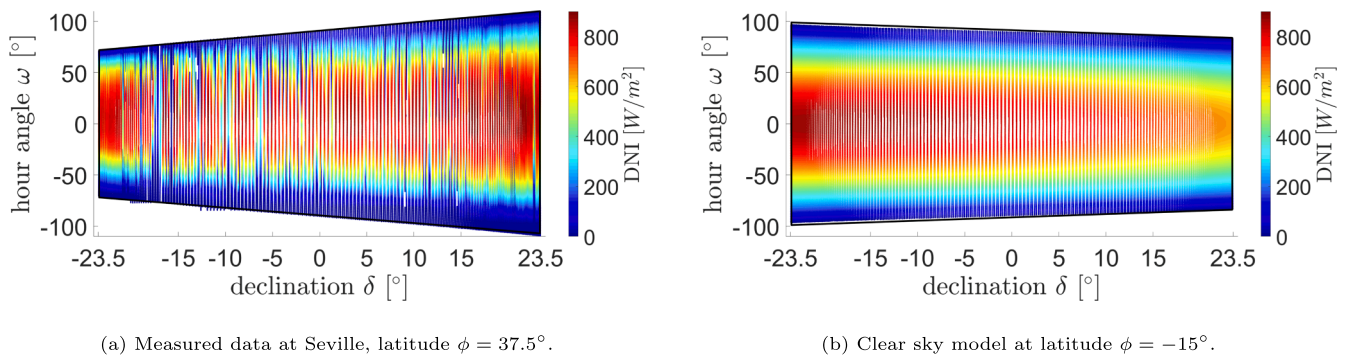


Fig. 4. Annual sun path in the equatorial coordinate system for two locations on Earth with different latitude. For the solar irradiation, measured meteorological data from Seville in (a), and clear-sky meteorological data in (b) is used. The whole domain can perfectly be bounded by a trapezoid (black line). For a location exactly on the equator, the bounding trapezoid reduces to a rectangle.

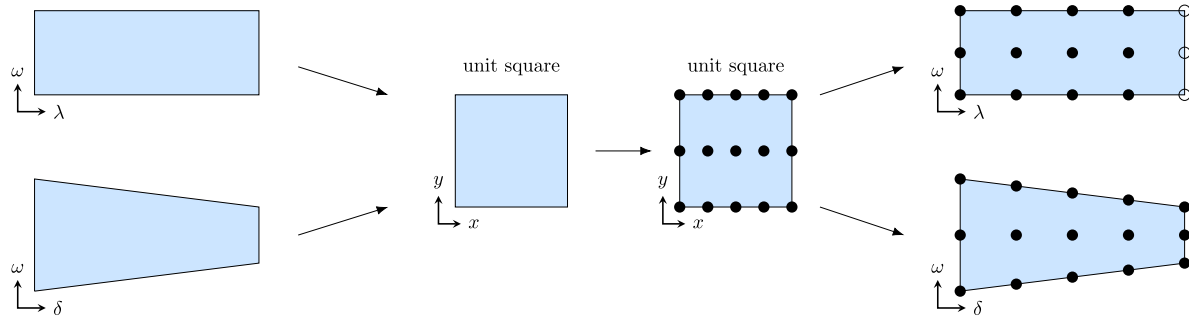


Fig. 5. Regular grid on a rectangular or a trapezoidal domain by transformation on a unit square.

- The *bilinear interpolation method* uses the four surrounding points to interpolate linearly in each dimension. Let $P_{00}(x_0, y_0)$, $P_{01}(x_0, y_1)$, $P_{10}(x_1, y_0)$, and $P_{11}(x_1, y_1)$ be the four surrounding grid points with $x_0 \leq x \leq x_1$ and $y_0 \leq y \leq y_1$, whereby their optical efficiency η_{00}^{sim} , η_{01}^{sim} , η_{10}^{sim} and η_{11}^{sim} is known. Thus, we first do linear interpolation in the x -direction using the ratio $\xi_x = \frac{x-x_0}{x_1-x_0}$,

$$\eta^{approx}(x, y_0) = (1 - \xi_x) \cdot \eta_{00}^{sim} + \xi_x \cdot \eta_{10}^{sim}, \tag{13}$$

$$\eta^{approx}(x, y_1) = (1 - \xi_x) \cdot \eta_{01}^{sim} + \xi_x \cdot \eta_{11}^{sim}. \tag{14}$$

Now, we interpolate between these new points in y -direction using the ratio $\xi_y = \frac{y-y_0}{y_1-y_0}$, such that we obtain

$$\eta^{approx}(x, y) = (1 - \xi_y) \cdot \eta^{approx}(x, y_0) + \xi_y \cdot \eta^{approx}(x, y_1). \tag{15}$$

- The *spherical linear interpolation (SLERP)* corresponds to a bilinear interpolation on a sphere (Shoemake, 1985). Thus, again we first do linear interpolation in the x -direction to approximate the efficiency for the two points $P_{x0}(x, y_0)$ and $P_{x1}(x, y_1)$, using the ratio $\xi_x = \frac{x-x_0}{x_1-x_0}$,

$$\eta^{approx}(x, y_0) = \frac{\sin((1 - \xi_x) \cdot \theta_{x0})}{\sin(\theta_{x0})} \cdot \eta_{00}^{sim} + \frac{\sin(\xi_x \cdot \theta_{x0})}{\sin(\theta_{x0})} \cdot \eta_{10}^{sim}, \tag{16}$$

$$\eta^{approx}(x, y_1) = \frac{\sin((1 - \xi_x) \cdot \theta_{x1})}{\sin(\theta_{x1})} \cdot \eta_{01}^{sim} + \frac{\sin(\xi_x \cdot \theta_{x1})}{\sin(\theta_{x1})} \cdot \eta_{11}^{sim}, \tag{17}$$

where $\theta_{x0} = \arccos \left\langle \left(\begin{matrix} x_0 \\ \eta_{00}^{sim} \end{matrix} \right), \left(\begin{matrix} x_1 \\ \eta_{10}^{sim} \end{matrix} \right) \right\rangle$ and $\theta_{x1} = \arccos \left\langle \left(\begin{matrix} x_0 \\ \eta_{01}^{sim} \end{matrix} \right), \left(\begin{matrix} x_1 \\ \eta_{11}^{sim} \end{matrix} \right) \right\rangle$ are the angles between the grid points. Then we interpolate between these two new points in y -direction using the ratio $\xi_y =$

$\frac{y-y_0}{y_1-y_0}$, such that we obtain

$$\eta^{approx}(x, y) = \frac{\sin((1 - \xi_y) \cdot \theta_{xy})}{\sin(\theta_{xy})} \cdot \eta^{approx}(x, y_0) + \frac{\sin(\xi_y \cdot \theta_{xy})}{\sin(\theta_{xy})} \cdot \eta^{approx}(x, y_1), \tag{18}$$

where $\theta_{xy} := \arccos(y_0 \cdot y_1 + \eta^{approx}(x, y_0) \cdot \eta^{approx}(x, y_1))$ is the angle between these new points.

- The *bicubic interpolation method* uses cubic splines, which results in a smoother interpolation surface (Keys, 1981). On the basis of 16 simulation points at $\{x_{-1}, x_0, x_1, x_2\} \times \{y_{-1}, y_0, y_1, y_2\}$ and their according optical efficiency η^{sim} , the interpolated efficiency in the cell $[x_0, x_1] \times [y_0, y_1]$ can be written as

$$\eta^{approx}(x, y) = \sum_{i=0}^3 \sum_{j=0}^3 a_{ij} x^i y^j. \tag{19}$$

For finding the 16 coefficients a_{ij} , a linear equation system must be solved, which considers the derivatives in x and y direction, and mixed partial derivatives of the optical efficiency. Consider that the quality of the solution for cells at the border get worse, as there are less interpolation points available, such that the method somehow reduces to a bilinear interpolation.

4.2. Interpolation on a non-regular grid

Higher degrees of polynomials on a regular grid lead to oscillations, which is known as Runge’s phenomenon. This effect can be avoided using a non-regular grid. For the choice of the interpolation points the zeros of orthogonal polynomials are used, as e.g. Legendre polynomials $P_{n+1}(x) = \frac{2n+1}{n+1} \cdot x \cdot P_n(x) - \frac{n}{n+1} \cdot P_{n-1}(x)$ with $P_0(x) = 1$ and $P_1(x) = x$. The zeros of the $(n + 1)$ -th Legendre polynomial are given as tabulated data or can be approximated by

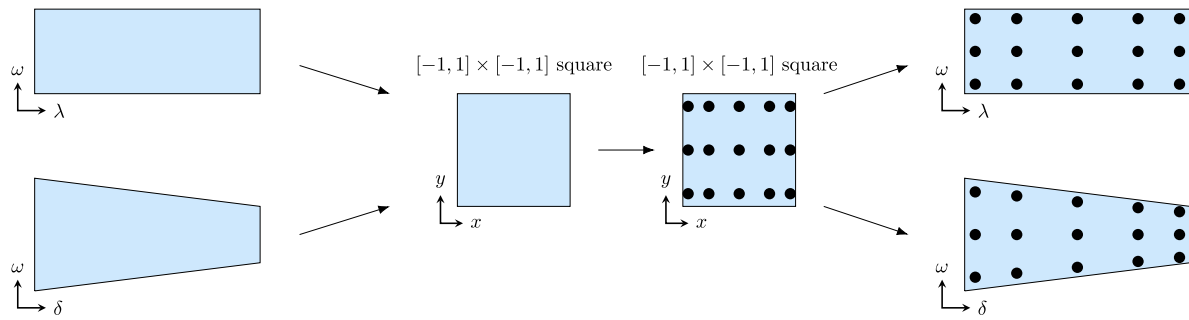


Fig. 6. Non-regular grid on a rectangular or a trapezoidal domain by transformation on a $[-1, 1] \times [-1, 1]$ square.

$$x_k^{Leg,approx} = \cos\left(\frac{4(k+1)-1}{4(n+1)+2}\pi\right) \in [-1, 1], \quad k = 0, \dots, n. \quad (20)$$

To apply the approximation, the rectangular or trapezoidal region of the domain is transformed to the $[-1, 1] \times [-1, 1]$ square, see Fig. 6. The $n \times m$ grid points are chosen as the zeros of the orthogonal polynomials in (20).

Let $\eta_{ij}^{sim} := \eta^{sim}(x_i^{Leg}, y_j^{Leg})$ be the simulated optical efficiency at the grid points (x_i^{Leg}, y_j^{Leg}) for $i = 1, \dots, n$ and $j = 1, \dots, m$. Then the optical efficiency can be approximated by a polynomial in the Lagrange form,

$$\eta^{approx}(x, y) = \sum_{i=0}^n \sum_{j=0}^m \eta_{ij}^{sim} \cdot L_{i,n}(x) \cdot L_{j,m}(y), \quad (21)$$

with Lagrangian polynomials

$$L_{i,n}(x) = \prod_{\substack{k=0 \\ k \neq i}}^n \frac{x - x_k^{Leg}}{x_i^{Leg} - x_k^{Leg}} \quad \text{and} \quad L_{j,m}(y) = \prod_{\substack{k=0 \\ k \neq j}}^m \frac{y - y_k^{Leg}}{y_j^{Leg} - y_k^{Leg}}. \quad (22)$$

5. Case study

In the following, the presented approximation methods are used to investigate the quality of the approximated efficiency in the ecliptic and equatorial coordinate systems. In Fig. 7 we visualize the efficiency η throughout a full year for a power plant with a cavity receiver and northern heliostat field (*PS10*), and a power plant with external receiver and a surrounding heliostat field (*Gemasolar*). Despite the different configurations of the two central receiver systems, the efficiency shows a similar behavior: The efficiency during winter months is very low in the morning and evening hours. During summer months, the power plant configurations start and end a day with moderate efficiency and reach high efficiency at midday. But there are also small differences: For *Gemasolar*, the difference between winter and summer months is more significant, compared to *PS10*. Throughout the year *PS10* consistently reaches higher efficiency values than *Gemasolar*. Especially in winter *PS10* shows higher efficiencies throughout the day. The reason for this observation lies in the different density of the two heliostat fields.

In the following case study we distinguish between these two heliostat field types, see Table 1 and Fig. 8. As meteorological data the direct normal solar irradiation from the EnergyPlus⁶ database for Seville is taken, see Fig. 1 (a).

For the simulation of single moments the raytracer *SunFlower* is used (Richter et al., 2018a), which was validated against the tools *SolTrace* and *Tonatiuh*. In *SunFlower*, the rays are equally distributed on the heliostat surface. The underlying technique is a mixed Monte Carlo ray

tracing method.

As the number of generated rays on the heliostat’s surface has a direct influence on the accuracy of the simulation, the settings of the raytracer are investigated for different altitudes of the sun, see Fig. 9. We are dealing with a ray tracing method which bases on random numbers to account for reflection errors due to sun shape and surface inaccuracies. Therefore each simulation (for the reference and for the interpolation) was done 30 times to detect the fluctuations in the solution. The reference value was simulated with 400 rays per square meter. In Fig. 9, the in red and blue shaded regions illustrate the fluctuation in dependency of the ray resolution.

For reaching an accuracy deviation of $\pm 0.05\%$ for a single simulation, in the following we use 50 rays per square meter for the *PS10* and 35 rays per square meter for the *Gemasolar*.

Next, the influence of the approximation methods on the accuracy of the annual simulation for the two test cases of *PS10* and *Gemasolar* are investigated. In Section 5.1 the different approximation methods are investigated for the optical annual energy production (ϵ_{AEP}), while in Section 5.2 the approximation accuracy for the received power for each timepoint of a year is considered with the root-mean-squared error (ϵ_{rmse}). Beside the ecliptic and equatorial coordinate system and the different methods, we need to investigate the number of simulated moments in each dimension.

5.1. Approximation of the received annual optical energy

As introduced in Section 2, for optical layout optimization which just considers the received annual optical energy of a power plant, an approximation method with low ϵ_{AEP} (3) is needed. In the following, we compare the accuracy of the five approximation methods in the ecliptic and equatorial coordinate system according to ϵ_{AEP} .

In Fig. 10 the ϵ_{AEP} error for each approximation method in dependency of the total number of simulated moments is shown. Here we just show a selection of the best combinations of simulated moments in x and y direction. It can be seen that with a larger number of simulated moments in general the accuracy also increases. The disturbances of the convergence are likely due to the fact that we are using measured meteorological data in the test cases. Furthermore changing, even increasing, the number of simulated points in one dimension results in completely different and in some cases unfavorable point distributions for interpolation, which in turn may lead to skewed results.

The convergence to a low ϵ_{AEP} error depends on the approximation method as well as on the chosen coordinate system. Almost without exception the approximation methods deliver better results in the equatorial coordinate system than in the ecliptic coordinate system. Bilinear and bicubic interpolation show the worst results in almost all cases. Nearest neighbor and especially SLERP offer slightly better accuracy. However, for *PS10* and for *Gemasolar* the Lagrange interpolation in equatorial coordinate system shows the overall fastest and most stable convergence.

In the next step we need to choose the number of simulated moments for the Lagrange interpolation in each dimension on the non-regular

⁶ EnergyPlus weather file <https://energyplus.net/weather>

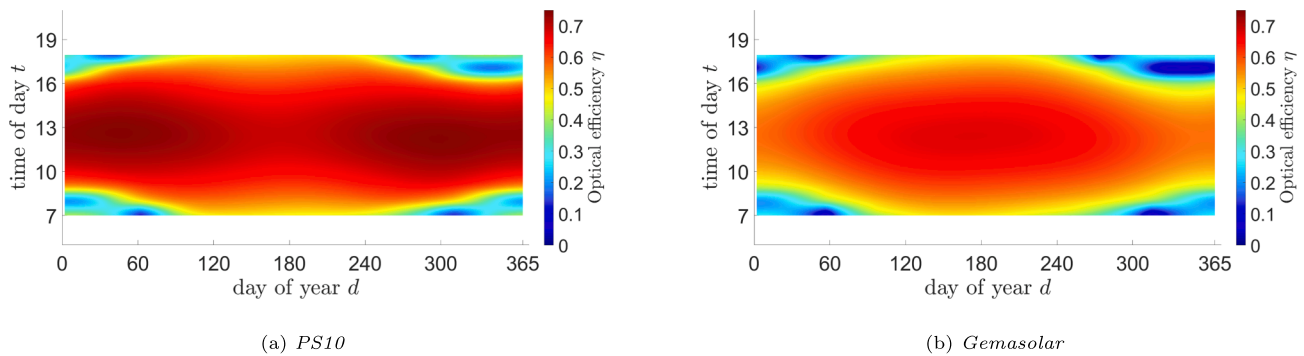


Fig. 7. Efficiency for all hourly daytime moments for the central receiver system *PS10* with cavity receiver and northern heliostat field (a), and for *Gemasolar* with external receiver and surrounding heliostat field (b).

Table 1

Power plant configuration of the *PS10* and the *Gemasolar* solar tower power plants, mostly from Schöttl et al. (2016).

Parameter	<i>PS10</i>	<i>Gemasolar</i>
Location	Seville (Spain)	Fuentes de Andalucía (Spain)
Longitude	6.25° W	5.32° W
Latitude	37.43° N	37.5° N
Number of heliostats	624	2650
Heliostat type	Sanlúcar 120	SENER HE35
Heliostat width	12.84 m	9.75 m
Heliostat height	9.45 m	12.30 m
Heliostat facet reflectance	0.88	0.93
Receiver shape	Cavity (width is 13.78 m)	Cylindrical (diameter is 8.5 m)
Receiver height	12 m	10.5 m
Receiver top position	115 m	126.5 m
Sun shape: Gaussian	2.35 mrad	2.35 mrad
Slope error	2.6 mrad	2.6 mrad
Tracking error	1.3 mrad	1.3 mrad

grid, as mentioned in Section 4. In Fig. 11 the accuracy of the Lagrange interpolation is shown in dependency of the total number of simulated moments and the selected number of points n in the declination angle δ dimension. For both power plants we get mostly good results by choosing $n = 4$. Alternatively choosing $n = 5$ also yields good results for both power plants. By fixing the number of points in one dimension we now can take a closer look at the results for this configuration.

As comparison, we compute the ϵ_{AEP} error for the popular *monthly*

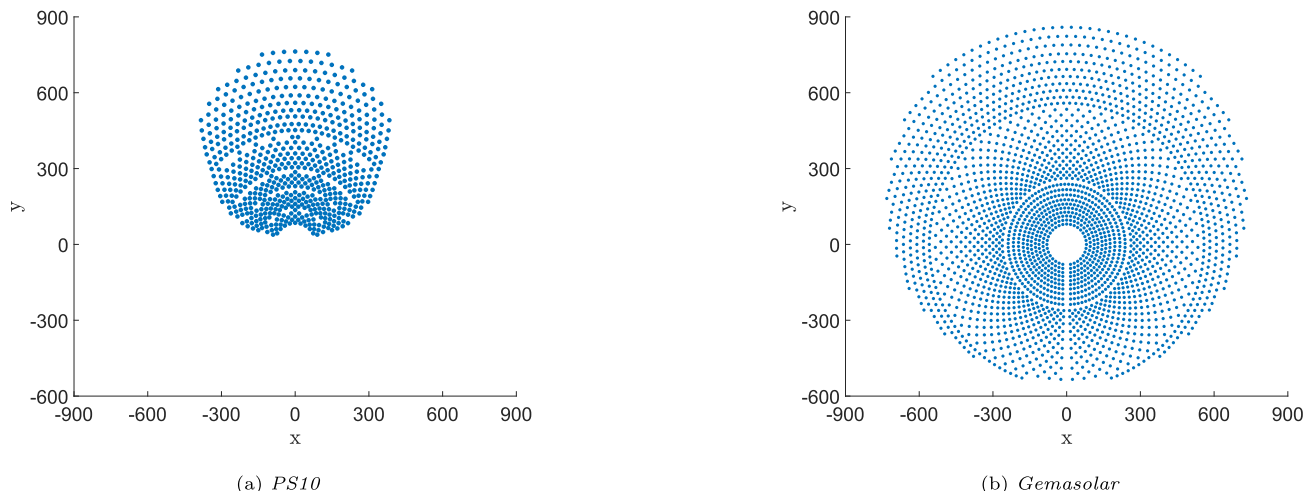


Fig. 8. Heliostat positions of the *PS10* power plant (a) and the *Gemasolar* power plant (b) in Seville, Spain.

nearest neighbor approximation using 87 simulated moments in a year. This method reaches an ϵ_{AEP} of 0.0798% for *PS10* and 0.3704% for *Gemasolar*. Using the Lagrange interpolation in the equatorial domain with 36 simulated moments ($n = 4$ and $m = 9$) for *PS10* or 44 simulated moments ($n = 4$ and $m = 11$) for *Gemasolar* the AEP error ϵ_{AEP} is similar to the *monthly nearest neighbor approximation*, see Table 2.

5.2. Approximation of received power for each hour in the year

For energetic layout optimization, which considers the thermal-electrical cycle of a power plant, an approximation method with low error at each time point in a year is needed, corresponding to a low ϵ_{rmse} (4). In the following, we compare the accuracy of the five approximation methods in the ecliptic and equatorial coordinate system according to ϵ_{rmse} .

In Fig. 12 the ϵ_{rmse} error for each approximation method in dependency of the total number of simulated moments is shown. Here we just show a selection of the best combinations of simulated moments in x and y direction. Again it can be seen that with a larger number of simulated moments also the error decreases. In this case the convergence is a lot more stable than for the ϵ_{AEP} , as ϵ_{rmse} is a more robust error function.

These plots show that the reduction of the ϵ_{rmse} error for an increasing number of simulated moments depends on the approximation method as well as on the chosen coordinate system. Again we can conclude that almost without exception the approximation methods deliver better results in the **equatorial coordinate system** than in the ecliptic coordinate system. Targeting ϵ_{rmse} , the Lagrange approximation and nearest neighbor interpolation show the worst results. SLERP, bilinear and

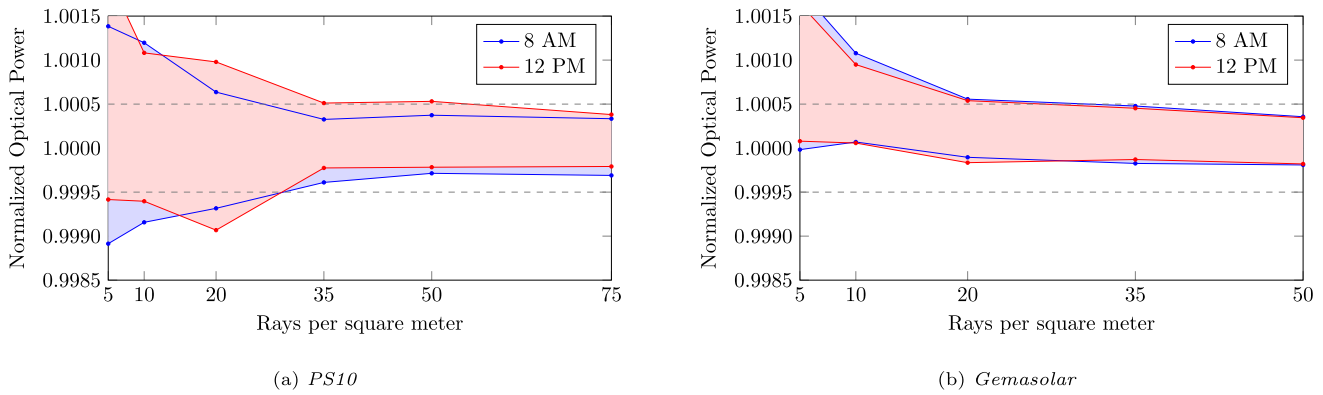


Fig. 9. Investigation of the ray resolution for *PS10* (a) and *Gemasolar* (b). The reference solution bases on 400 rays per square meter. At 21st of June, different altitudes of the sun are used to consider the influence of changing blocking and shading effects. Each simulation was done thirty times to account for fluctuations, illustrated by the shaded regions.

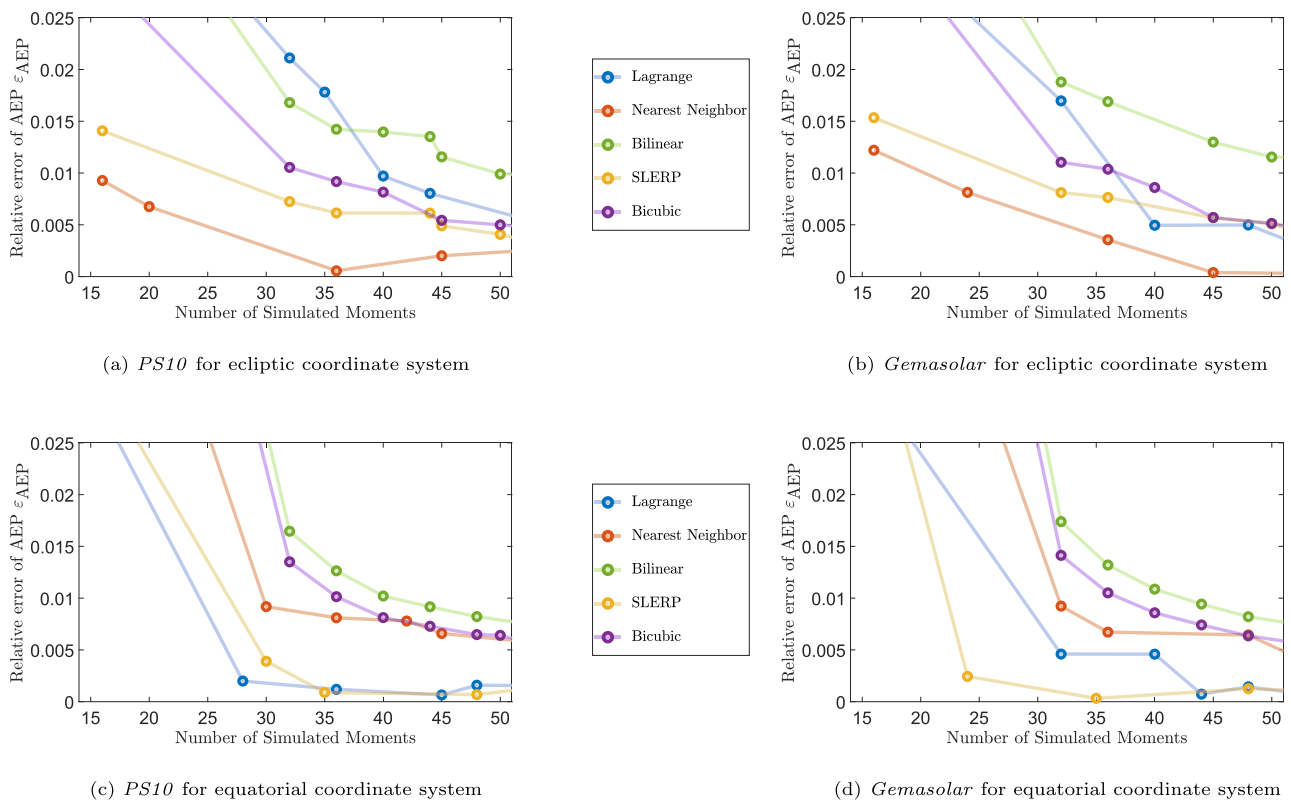


Fig. 10. Comparison of the different approximation methods in the ecliptic and equatorial coordinate system in dependency of the number of simulated moments.

bicubic interpolation perform similar, but in case of the equatorial domain, the **bicubic interpolation** yields the overall best results for *PS10* and *Gemasolar*.

In the next step we need to choose the number of simulated moments for the bicubic interpolation in each dimension on the grid, as mentioned in Section 4. In Fig. 13 the error of the bicubic interpolation is shown in dependency of the total number of simulated moments and the number of points n in the dimension of the declination angle δ . For both power plants the best results are clearly reached by choosing $n = 4$ points in direction of the declination angle δ . Using this confinement, we can take a closer look at the results.

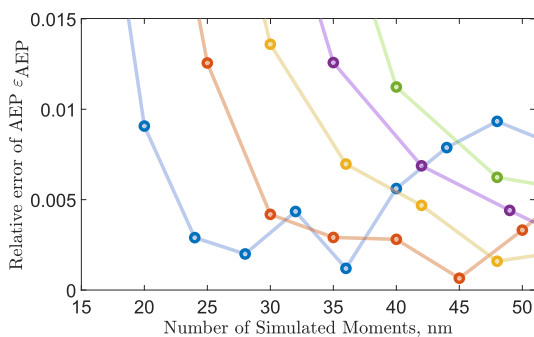
As comparison, we compute the ϵ_{rmse} error for the popular *monthly nearest neighbor approximation* using 87 simulated moments in a year. This method reaches an ϵ_{RMSE} of $4.282 \cdot 10^5$ for *PS10* and $1.912 \cdot 10^6$ for *Gemasolar*. Using the bicubic interpolation in the equatorial domain

with 36 simulated moments ($n = 4$ and $m = 9$) we get a lower RMSE error ϵ_{rmse} compared to the *monthly nearest neighbor approximation* while using two to three times less points, see Table 3.

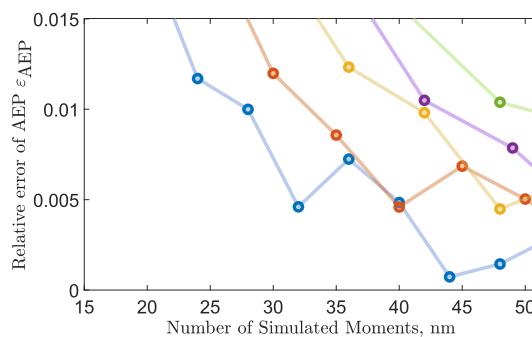
The goal of a low RMSE error ϵ_{rmse} is to reach an accurate approximation of the received optical power at each instance of time in the year. Thus, in Fig. 14 the error of the power $P^{\text{approx}}(d, t)$ for the whole year is visualized.

The bicubic interpolation in the equatorial domain shows for both power plants throughout the whole temporal domain a high accuracy. Only close to sunrise and sunset the method delivers some inaccuracies. This disadvantage has no strong influence on the quality of the solution due to a low solar irradiation at these moments.

For the *monthly nearest neighbor approximation* its monthly structure is clearly visible (just one day in each month is regarded for simulation). Besides similar inaccuracy close to sunrise and sunset, another weakness

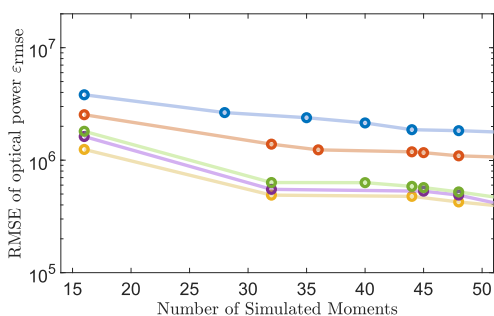


(a) *PS10* with Lagrange interpolation in equatorial coordinate system.

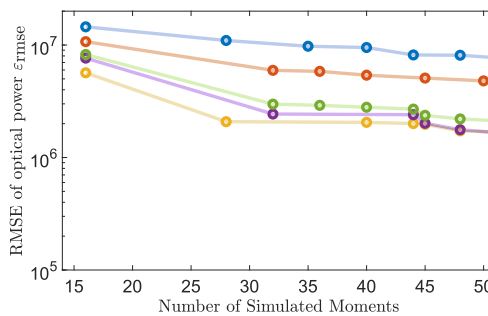


(b) *Gemasolar* with Lagrange interpolation in equatorial coordinate system.

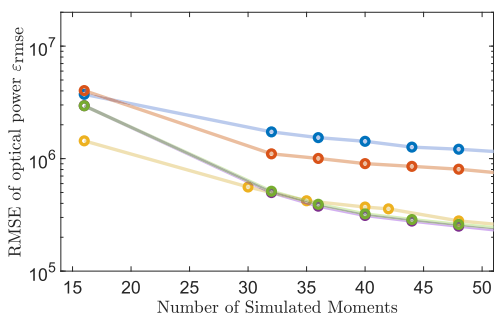
Fig. 11. Approximation results for selected point combinations using the Lagrange approximation, where n is the number of simulated moments for the declination angle δ , and m the number of simulated moments for the hour angle ω .



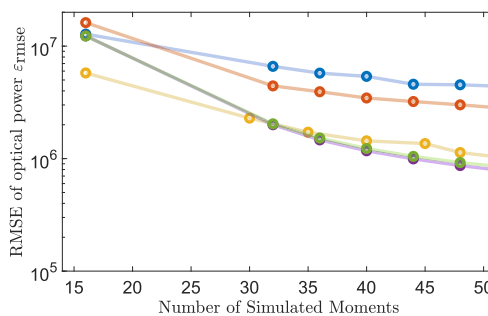
(a) *PS10* for ecliptic coordinate system



(b) *Gemasolar* for ecliptic coordinate system



(c) *PS10* for equatorial coordinate system



(d) *Gemasolar* for equatorial coordinate system

Fig. 12. Comparison of the different approximation methods in the ecliptic and equatorial coordinate system in dependency of the number of simulated moments.

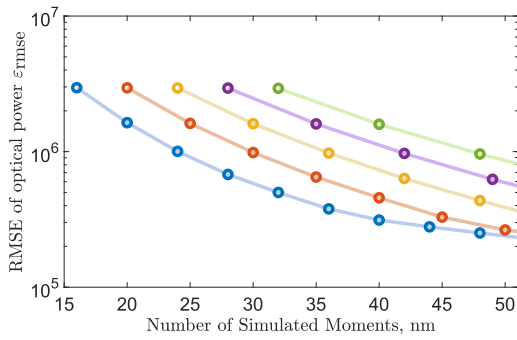
of the *monthly nearest neighbor approximation* are high inaccuracies in-between two simulated days. In Fig. 14 (c) and (d) it can be seen, that the error of the monthly nearest neighbor approximation is non-symmetric. This comes due to some symmetry assumptions of the method that just seven out of twelve months are simulated (Pitz-Paal et al., 2011). The results would be better if all months are used, which on the other hand would mean a strong increase of the number of needed simulation points.

As seen in Table 3 and comparing the plots of Fig. 14 (a) with (c), and (b) with (d) directly, the overall error is smaller using the bicubic interpolation method while needing less than half the number of simulated moments.

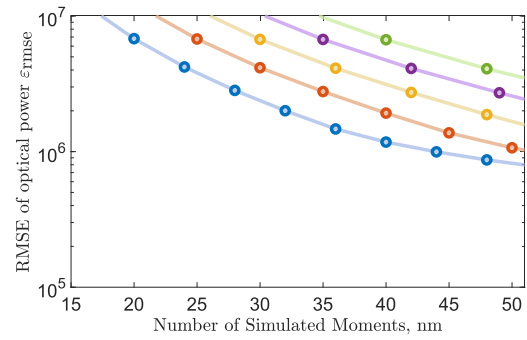
5.3. Discussion of the results

As main result of this case study we find that the quality of the approximation methods depends on the choice of the underlying coordinate system. Almost without exception the approximation methods deliver the best results in the equatorial coordinate system, which can be seen in Fig. 10 and in Fig. 12.

Aside from the coordinate system, the results show that the approximation method shall be chosen depending on the target function. We found out that a Lagrange approximation with $n = 4$ simulated moments for the declination angle δ yields the best results when approximating the received annual optical energy (according to ϵ_{AEP}), see Figs. 10 and 11. When focussing on the power for each individual hour of a year (according to ϵ_{rmse}), a bicubic interpolation with $n = 4$ simulated moments for the declination angle δ gives the best results, see

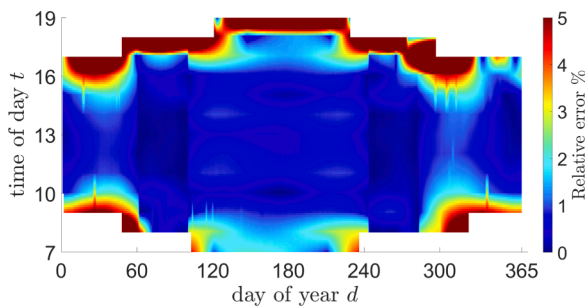


(a) *PS10* with bicubic interpolation in equatorial coordinate system.

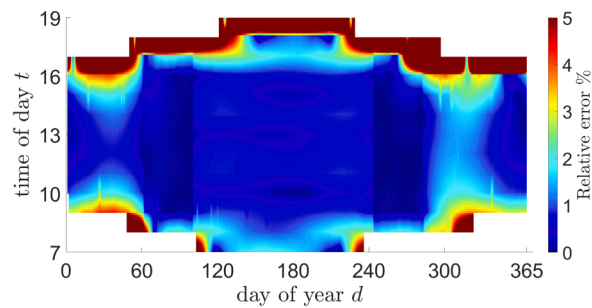


(b) *Gemasolar* with bicubic interpolation in equatorial coordinate system.

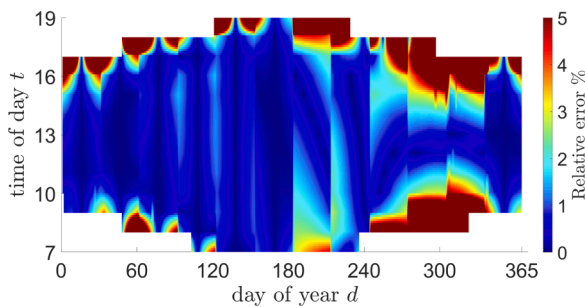
Fig. 13. Approximation results for selected point combinations using the bicubic interpolation in the equatorial coordinate system. n is the number of simulated moments in x -direction, which is the declination angle δ .



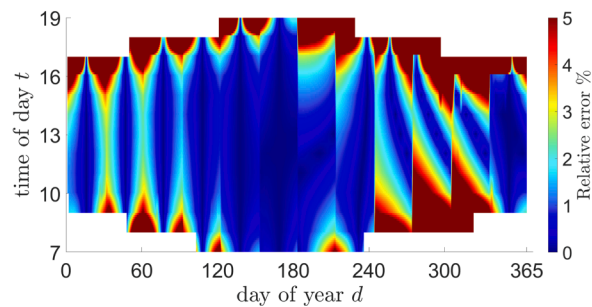
(a) *PS10* with bicubic interpolation in equatorial domain with $40 = 4 \times 10$ simulated moments.



(b) *Gemasolar* with bicubic interpolation in equatorial domain with $40 = 4 \times 10$ simulated moments.



(c) *PS10* with monthly nearest neighbor approximation.



(d) *Gemasolar* with monthly nearest neighbor approximation.

Fig. 14. Relative error $\frac{|p^{sim}(d,t) - p^{approx}(d,t)|}{p^{sim}(d,t)}$ for all hourly moments. The bicubic interpolation in equatorial coordinate system is used to compare against the monthly nearest neighbor approximation based on 87 simulated moments (c) and (d).

Figs. 12 and 13.

The case study also shows that these observations hold even for different power plant configurations. For *PS10* and the chosen equatorial coordinate system the Lagrange approximation delivers an accuracy of 99.566% for the received annual optical energy by just using 32 simulation points. The same method applied to *Gemasolar* delivers an accuracy of 99.54%, see Table 2.

In comparison to existing approaches as e.g. the monthly nearest neighbor approximation (Pitz-Paal et al., 2011), we can reduce the number of needed simulations from 87 to 36 or even less, while achieving similar accuracy and even lower RMSE, see Tables 2,3. So using the here-in developed approximation method the whole simulation can be speed up by a factor of up to three.

6. Conclusion

In this work a new approximation method for the annual simulation of solar central receiver systems is developed. Two coordinate systems are considered in which five approximation methods are investigated and compared against existing methods. A transformation into the equatorial and ecliptic coordinate system is used, such that the approximation methods are independent from the considered location on Earth. For power plants in the sub-tropic region, the monthly nearest neighbor approximation needs to be adapted as the symmetry of months changes, while our approach in the ecliptic and equatorial coordinate system does not need any adaptations. In a case study it is shown that the number of simulation points in a year can be reduced by using different coordinate systems and approximation methods while maintaining

Table 2
Comparison of the approximation results for different resolutions for the Lagrange interpolation in the equatorial coordinate system and the *monthly nearest neighbor approximation*.

Approximation method	Domain	Number of simulated moments	<i>PS10</i> ϵ_{AEP}	<i>Gemasolar</i> ϵ_{AEP}
Lagrange interpolation	Equatorial domain	24	0.289%	1.169%
Lagrange interpolation	Equatorial domain	28	0.199%	0.999%
Lagrange interpolation	Equatorial domain	32	0.434%	0.46%
Lagrange interpolation	Equatorial domain	36	0.120%	0.724%
Lagrange interpolation	Equatorial domain	40	0.561%	0.484%
Lagrange interpolation	Equatorial domain	44	0.788%	0.073%
Lagrange interpolation	Equatorial domain	48	0.933%	0.144%
Monthly nearest neighbor	Temporal domain	87	0.0798%	0.3704%

Table 3
Comparison of the approximation results for different resolutions for the bicubic interpolation in the equatorial coordinate system and the *monthly nearest neighbor approximation*.

Approximation method	Domain	Number of simulated moments	<i>PS10</i> ϵ_{rmse} [W]	<i>Gemasolar</i> ϵ_{rmse} [W]
Bicubic interpolation	Equatorial domain	24	10.03·10 ⁵	4.206·10 ⁶
Bicubic interpolation	Equatorial domain	28	6.781·10 ⁵	2.826·10 ⁶
Bicubic interpolation	Equatorial domain	32	4.992·10 ⁵	2.001·10 ⁶
Bicubic interpolation	Equatorial domain	36	3.778·10 ⁵	1.468·10 ⁶
Bicubic interpolation	Equatorial domain	40	3.124·10 ⁵	1.175·10 ⁶
Monthly nearest neighbor	Temporal domain	87	4.282·10 ⁵	1.912·10 ⁶

similar accuracy compared to existing methods. For the two power plants *PS10* and *Gemasolar* it is shown that an accuracy of more than 99.7% for the received power can be reached, while reducing the number of needed simulation points by factor two to three. Due to the adjustable resolution of the approximation method in fine steps, the here-in developed methods can be used for a wide range of applications, e.g. for fast simulations (32 simulation points deliver an accuracy of about 99.5%) or highly accurate resolutions (carefully chosen 44 to 45 simulation points deliver an accuracy of about 99.9%).

Using this methodology, very detailed annual simulations of solar central receiver systems can be performed within reasonable time. This approach can be used for heliostat field layout optimizations with dynamic optimization using a multilayer structure with increasing accuracy of the simulation model. In such a way faster optimizations are possible which will lead to better optimized layouts.

Future work. Points near the boundaries of the hour angle dimension, corresponding to low sun elevation, show extreme fluctuations in

efficiency as the blocking and shading changes rapidly. A rectangle or trapezoid was used to fully enclose the domains by theoretical boundaries. In practice it might be beneficial to avoid simulation at these boundaries when approximating. One approach is to use a non-regular grid as we do for the Lagrange interpolation, which does not simulate the boundaries of the domain, and investigate this type of point distribution with other approximation methods. We can also prune boundary points in the hour angle dimension to retrieve a *core-region* of the day. Here the idea is to focus the approximation on the region of the day where the majority of electrical power is generated. This might allow a much quicker, while still reasonably precise, approximation. Beside the investigation of the interpolation method with more power plant setups including even larger power plants in different regions of the world, it might also be interesting to investigate the annual performance of single heliostats on certain positions, which can later be used for the selection of heliostat positions in the field layout optimization.

Declaration of Competing Interest

The authors declare that they have no known competing financial interests or personal relationships that could have appeared to influence the work reported in this paper.

References

Ahlbrink, N., Belhomme, B., Flesch, R., Maldonado Quinto, D., Rong, A., Schwarzbözl, P., 2012. Stral: Fast ray tracing software with tool coupling capabilities for high-precision simulations of solar thermal power plants. In: Proceedings of the SolarPACES 2012 Conference, pp. 1–8.

Armstrong, P., Izygon, M., 2014. An innovative software for analysis of sun position algorithms. Energy Procedia 49, 2444–2453.

Blanco, M.J., Amieva, J.M., Mancillas, A., 2005. The tonatuh software development project: An open source approach to the simulation of solar concentrating systems. In: ASME 2005 International Mechanical Engineering Congress and Exposition. American Society of Mechanical Engineers Digital Collection, pp. 157–164.

Grigoriev, V., Corsi, C., Blanco, M., 2016. Fourier sampling of sun path for applications in solar energy. In: AIP Conference Proceedings, vol. 1734. AIP Publishing, p. 020008.

Keys, R., 1981. Cubic convolution interpolation for digital image processing. IEEE Trans. Acoust. Speech Signal Process. 29 (6), 1153–1160.

Meeus, J.H., 1991. Astronomical Algorithms. Willmann-Bell, Incorporated.

Noone, C.J., Torrilhon, M., Mitsos, A., 2012. Heliostat field optimization: a new computationally efficient model and biomimetic layout. Sol. Energy 86 (2), 792–803.

Pitz-Paal, R., Botero, N.B., Steinfeld, A., 2011. Heliostat field layout optimization for high-temperature solar thermochemical processing. Sol. Energy 85 (2), 334–343.

Potter, D.F., Kim, J.-S., Khassapov, A., Pascual, R., Hetherington, L., Zhang, Z., 2018. Heliosim: An integrated model for the optimisation and simulation of central receiver csp facilities. In: AIP Conference Proceedings, vol. 2033. AIP Publishing, p. 210011.

Richter, P., Heiming, G., Lukas, N., Frank, M., 2018a. Sunflower: A new solar tower simulation method for use in field layout optimization. In: AIP Conference Proceedings, vol. 2033. AIP Publishing, p. 210015.

Richter, P., Tinnes, J., Schwarzbözl, P., Rong, A., Frank, M., 2018b. Efficient ray-tracing with real weather data. In: AIP Conference Proceedings, vol. 2033. AIP Publishing, p. 210014.

Richter, P., 2017. Simulation and Optimization of Solar Thermal Power Plants. PhD thesis. RWTH Aachen University.

Schöttl, P., Moreno, K.O., Bern, G., Nitz, P., et al., 2016. Novel sky discretization method for optical annual assessment of solar tower plants. Sol. Energy 138, 36–46.

Shoemake, K., 1985. Animating rotation with quaternion curves. In: ACM SIGGRAPH computer graphics, volume 19 (3). ACM, pp. 245–254.

Urban, S.E., Kenneth Seidelmann, P., 2013. Explanatory Supplement to the Astronomical Almanac. University Science Books.

Wendelin, T., 2003. Soltrace: a new optical modeling tool for concentrating solar optics. In: ASME 2003 International Solar Energy Conference. American Society of Mechanical Engineers, pp. 253–260.

Yahaoui, I., 2016. Specifications of Photovoltaic Pumping Systems in Agriculture: Sizing, Fuzzy Energy Management and Economic Sensitivity Analysis. Elsevier.